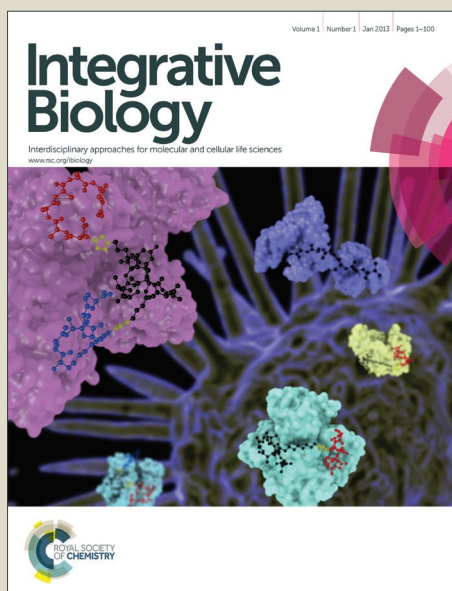


Integrative Biology

Accepted Manuscript



This is an *Accepted Manuscript*, which has been through the Royal Society of Chemistry peer review process and has been accepted for publication.

Accepted Manuscripts are published online shortly after acceptance, before technical editing, formatting and proof reading. Using this free service, authors can make their results available to the community, in citable form, before we publish the edited article. We will replace this *Accepted Manuscript* with the edited and formatted *Advance Article* as soon as it is available.

You can find more information about *Accepted Manuscripts* in the [Information for Authors](#).

Please note that technical editing may introduce minor changes to the text and/or graphics, which may alter content. The journal's standard [Terms & Conditions](#) and the [Ethical guidelines](#) still apply. In no event shall the Royal Society of Chemistry be held responsible for any errors or omissions in this *Accepted Manuscript* or any consequences arising from the use of any information it contains.

Insight Statement

The cell mixer microbio reactor array (CM-MBA) presented in this paper combines the ability to rapidly establish co-culture models in a high-throughput, programmable fashion, with the additional advantage of maintaining mixed cell populations in culture under perfused medium to explore paracrine factor impacts, representing a promising new tool for directing multi-cellular tissue formation for tissue engineering applications.



Integrative Biology

ARTICLE

Stoichiometric control of live cell mixing to enable fluidically-encoded co-culture models in perfused microbio reactor arrays

P. Occhetta,^{a,b} N. Glass,^a E. Otte,^{a,d} M. Rasponi,^b and J.J. Cooper-White^{a,c,d,*}

Received 00th January 20xx,
Accepted 00th January 20xx

DOI: 10.1039/x0xx00000x

www.rsc.org/

In vivo, tissues are maintained and repaired through interactions between the present (different) cell types, which communicate with each other through both the secretion of paracrine factors and direct cell-cell contacts. In order to investigate and better understand this dynamic, complex interplay among diverse cell populations, we must develop new *in vitro* co-culture strategies that enable us to recapitulate such native tissue complexity. In this work, a microfluidic mixer based on a staggered herringbone design was computationally designed and experimentally validated that features the ability to mix large, non-diffusive particles (i.e. live cells) in a programmed manner. This is the first time that the herringbone mixer concept has been shown to effectively mix particles of the size range applicable to live cells. The cell mixer allowed for sequentially mixing of two cell types to generate reverse linear concentration co-culture patterns. Once validated, the mixer was integrated into a perfused microbio reactor array as an upstream module to deliver mixed cells to five downstream culture units, each consisting of ten serially-connected circular microculture chambers. This novel cell mixer microbio reactor array (CM-MBA) platform was validated through the establishment of spatio-temporally tunable osteogenic co-culture models, investigating the role of pre-osteoblastic cells (SAOS2) on human mesenchymal stem cells (hMSCs) commitment to an osteogenic endpoint. An increase on expression of alkaline phosphatase in sequential (downstream) chambers, consistent with the initial linear distribution of SAOS2, suggests not only osteoblastic cell-driven hMSCs induction towards the osteogenic phenotype, but also the importance of paracrine signaling. In conclusion, the cell mixer microbio reactor array combines the ability to rapidly establish cell co-culture models in a high-throughput, programmable fashion, with the additional advantage of maintaining cells in culture under perfused medium to explore paracrine factor impacts, representing a promising new tool for directing multi-cellular tissue formation for tissue engineering applications.

Introduction

In vivo, cell behaviors within tissues are influenced by dynamic variations (temporally and spatially) in physical and chemical cues, derived from the surrounding extracellular matrix (ECM) and neighboring cells. Tissues are composed of many repeats of so-called functional units or niches, which themselves are composed of multiple cell types that engage in highly specific interactions with each other, through both secreted soluble factors (paracrine signaling) and direct cell-cell contact (through cell adhesion molecules). These inter-cellular communications play a key role in defining the maintenance of cell phenotype, the commitment towards specific cell fates^{1,2},

and even the patterning and cell type localization observed within tissue functional units or niches. Due to the substantial differences in cellular microenvironments, even within a niche (for example, the perivascular niche), removing cells from such a controlled microenvironment and culturing them separately can lead to substantial differences in behavior and function. To study the dynamic interplay of diverse cell types and their respective roles in determining tissue function, responses to injury and mechanisms of repair *in vitro* is however difficult, as we must develop *in vitro* co-culture strategies that enable one to recapitulate such native complexity. To date, most co-culture techniques are based on the use of transwell systems, which relies on the exploitation of a permeable membrane to keep cells physically separated, while allowing soluble factor-based communications. Although exploited in several fields of cell biology (i.e. osteoblast-stem cells³, neurons-astrocytes⁴, cardiac fibroblast-cardiomyocytes⁵ co-cultures), these approaches generally lack in accurately recapitulating the complexity of the native multicellular environment. Indeed, they mainly consist in macroscale culture systems in which cells are manually grown under static conditions and where direct cell-cell physical interactions are inhibited⁶. In addition, these methods are time-consuming, allow for the testing of

^a Australian Institute of Bioengineering and Nanotechnology, The University of Queensland, Brisbane, QLD, Australia. E-mail: j.cooperwhite@uq.edu.au

^b Department of Electronics, Information and Bioengineering, Politecnico di Milano, Milano, Italy.

^c School of Chemical Engineering, The University of Queensland, Australia 4072.

^d Biomedical Manufacturing, Manufacturing Flagship, CSIRO, Clayton, Victoria, Australia, 3169.

* - corresponding author (j.cooperwhite@uq.edu.au)

Electronic Supplementary Information (ESI) available: [details of any supplementary information available should be included here]. See DOI: 10.1039/x0xx00000x

only a few conditions at a time and offer a limited control over the dynamics of cell communication processes.

Microfabrication technologies have more recently been exploited to downscale co-culture environments to better match the typical length (10's to 100's microns) and timescales (seconds to minutes) of cellular interactions^{7, 8}. A number of approaches have been utilized to generate highly organized co-culture models through spatially compartmentalizing different cell populations within defined microenvironments. These approaches have relied on the use of geometrical constraints⁹, semi-permeable membranes¹⁰, micropatterning strategies¹¹⁻¹⁴ or pneumatic/hydraulic valves^{7, 8}. The development of microfluidic microreactors for cell culture have enabled the combination of the abovementioned advantages of miniaturization with innovative, dynamic and high-throughput strategies for tailoring biomimetic cellular environments¹⁵. The continuous perfusion of cell culture media within such devices has indeed demonstrated more uniform and controlled culture conditions than traditional static approaches, providing constant dilution of catabolites and a stable supply of nutrients^{6, 16, 17}. Moreover, the ability to handle cells and fluids within precise spatial configurations provides the possibility to screen several culture parameters in a high-throughput fashion¹⁸.

Although many microfluidic strategies have been developed to generate and deliver temporally and spatially variant mixtures of soluble factors (e.g. small molecules such as growth factors)¹⁹⁻²², the ability to stoichiometrically mix larger (non-soluble) particles (e.g. cells) with high fidelity into defined ratios is limited, due principally to the lack of convective mixing in standard microchannel flows²³. To overcome the diffusive mixing limitations of microfluidic devices, a few technical solutions have been proposed. These are based on either active approaches, relying on external energy inputs,^{24, 25} or passive manipulation of fluid flows²⁶⁻²⁹. Among the latter, methods based on 'split and recombine'²⁶ and chaotic mixing²⁷ strategies that rely on the consecutive division and recombination of the fluid streamlines into multiple sub-portions, thus decreasing the effective diffusion length among adjacent streamlines, have proven most useful. In particular, chaotic mixers have become widespread due to their straightforward implementation on most microfluidic layouts without the need for significant device redesign, but just the addition of staggered herringbones (HB) features on top of rectangular cross-sectional channels³⁰. However, to date, HB features have not been utilized to mix large non-diffusive particles, such as live cells.

In this work, we demonstrate the capability to mix suspensions of different cell types of varying sizes into predetermined stoichiometric ratios for subsequent co-culture through the implementation of chaotic mixing. We have designed and validated an innovative chaotic-based serial dilution generator (SDG) – or 'cell mixer' – optimized for the programmed mixing of cells in a linear concentration profile (0% - 100%, with steps 25%). The cell mixer was then integrated into a microfluidic device to generate spatially controlled co-culture models within five downstream arrayed culture units. The presented

cell mixer microreactor array (CM-MBA) platform combined the ability to establish co-culture models in a high-throughput and fully automated fashion, with the advantage of culturing cells within a perfused microenvironment for extended culture. Furthermore, the integration of serially-connected culture chambers allowed for the investigation of the dependence of different cell ratios and paracrine signaling on co-culture outcomes. The versatility and potential of the detailed CM-MBA platform was validated through the establishment of an osteogenic co-culture model, aimed at investigating the influence of pre-osteoblastic cells on human mesenchymal stromal cell commitment to an osteogenic lineage.

Materials and methods

Cell mixer: design and computational validation

The cell mixer, based on a chaotic SDG element, was implemented to mix cells with a split-and-recombine scheme, achieving programmed concentration ratios. The mixer comprises a symmetric microfluidic network (channel size of 240x100µm in width and height, respectively)¹⁹, integrated with staggered herringbone (HB) grooves to increase the mixing through vortex formation^{27, 31}. The HB features, having the same width as the main fluidic channels, were designed to be 60µm long and 36µm high and orientated of a 45° angle (y-angle) with respect to the long axis of the channel. The elementary mixing building block (HB unit) consisted of a 1.72mm long channel, embedding twelve HB features, reversing their orientation every half cycle (see Table 1).

Table 1. HB mixing unit dimensions

Channel width [µm]	240
Channel height [µm]	100
Unit length [µm]	1720
Ratio of HB half height (a)	0.18
Degree of asymmetry (p)	2/3
HB width [µm]	60
HB height [µm]	36
Distance b/w HB [µm]	60
HB number	6+6
HB y-angle [°]	45

The minimum number of repeating HB units required to ensure mixing of both soluble (i.e. growth factors, $D=8,4 \times 10^{-11}$ m²/sec) and non-diffusive species (e.g. cells) was identified through finite element analysis-based Computational Fluid Dynamic models (CFD, Comsol Multiphysics). Analyses were performed on 3D geometrical models of HB grooved channels consisting of ten repeating HB units, using rectangular channels with the same length as controls. Geometries were discretized through a tetrahedral mesh scheme, consisting of about 1061×10^3 and 110×10^3 elements, in the case of presence and absence of HBs, respectively (Fig.1a). The flow field was computed by solving stationary Navier–Stokes equations for incompressible flow, setting density and viscosity equal to

1000 kg/m³ and 0.890 cP, respectively³¹. Uniform velocity profiles were applied to inlets, corresponding to Reynolds numbers (Re) ranging from 0.01 and 1 (Q_{in}=0.1–10 μl/min), while a zero pressure condition was set to the outlet. A no-slip boundary condition was applied to walls. Convergence criterion was satisfied when the normalized residuals for the velocities fell below 1×10⁻⁶.

The mixing efficacy was evaluated along cross sections of channels by means of the Transport of Diluted Species application model. Fig. 1a and b shows the trend of concentrations along both HB and control channels corresponding to Re 0.01 and 1, respectively. A range of Re between 0.01 and 1 was investigated, as this range was considered to maximize cell viability in terms of possible effects of shear stress on cells during seeding procedures.

Starting from concentration values along channels, an index of mixing efficiency (ME) was computed as it follows³²:

$$ME = 1 - \frac{1}{N} \sum_{i=1}^N \left(\frac{c_i - \bar{c}}{\bar{c}} \right)^2$$

where c_i is the mass fraction of species at the point i th belonging to a cross-section of the channel, and \bar{c} is the average mass fraction of species. Concentration of species was allowed to range from 0 to 1, and \bar{c} was set equal to 0.5. The ME was evaluated at the outlet of each repeated unit (Fig. 1c and d). The mixing was considered complete for ME higher than 0.95, n being the minimum number of repeated units required for achieving efficient mixing. Considering soluble factors, the presence of HB structures significantly enhanced the mixing at both Re numbers (Fig. 1c).

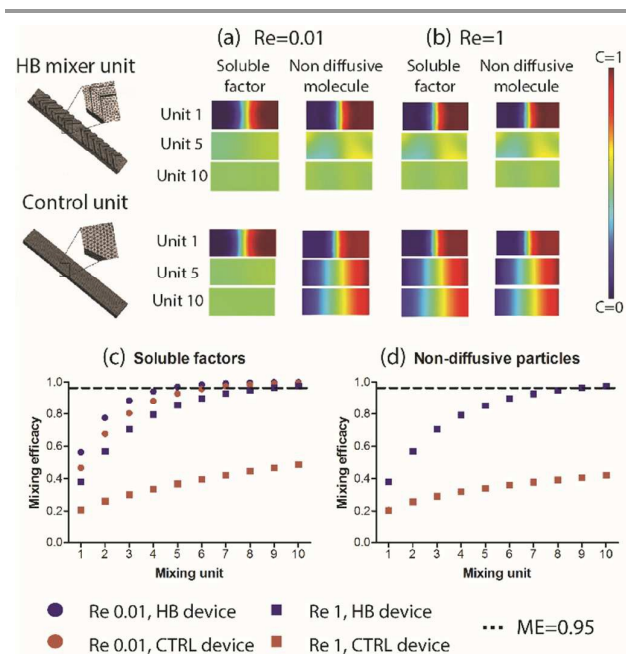


Fig. 1 The mixing efficiency of both HB mixer and control units was evaluated through CFD simulations for both soluble and non-diffusive species. Re=0.01 (a) and 1 (b). An index of mixing efficiency was calculated (ME) as function of repeated units (c, d). The

mixing was considered complete for ME higher than 0.95, n being the minimum number of repeated units required for achieving efficient mixing.

For low Re (0.01), the mixing is achieved in both HB and control channels, after five and six repeated units, respectively. Conversely, at Re 1 no mixing occurs in the purely diffusive control channel, while the addition of HBs allowed for complete mixing after eight units. Regarding non-diffusive particles (Fig. 1d), uniform mixing is achievable through the inclusion of at least eight HBs units, while no significant mixing was detectable in corresponding rectangular control channels at neither Re numbers.

Microfluidic platform design and fabrication

Upon computational optimization, the final chip layout (Fig. 2) was designed, integrating a three-level cell mixer. Due to the linear flow velocity not being uniform through the levels, the mixer was first dimensioned considering the lowest flow rate, namely characterizing the third level. Indeed, chaotic mixing efficacy has been shown to be higher for higher flow rate. Given that the minimum number of repeated HB units theoretically required in this most critical section to achieve complete mixing of non-diffusive particles (Fig. 1d) was eight, a safety margin was defined and the number of HB units was further increased at each SDG level, in accord with the decreases in flow rate along the symmetric network¹⁹. In detail, 17, 21 and 27 HB units were sequentially integrated on top of the fluidic channel in the three levels of the SDG, respectively. As described previously, dimensions and geometry of HB features were maintained equal to the computational model and each HB unit consisted of twelve HB features, changing their orientation every half cycle. Five downstream independent arrayed culture units were then implemented, each consisting in ten serially-connected circular culture chambers ($\Phi=1.63\text{mm}$, $h=100\mu\text{m}$)²² and integrated with a lateral seeding channel. Two secondary inlets (B1, B2) were finally included in the layout to facilitate the medium change operations¹⁷. For preliminary validation experiments, a supplementary version of the device was developed (see SI, Fig.S11), in which every outlet of the cell mixer was connected to a single rectangular culture chamber ($w3000 \times l6000 \times h100 \mu\text{m}$).

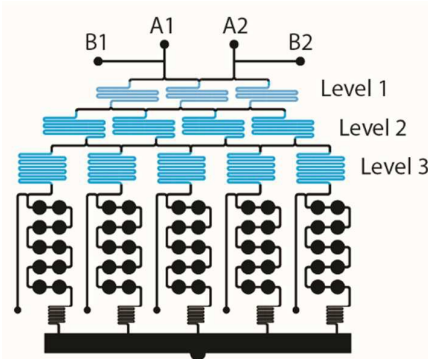


Fig. 2 A microbioreactor array for culturing cell co-culture models was designed consisting of (i) the previously validated cell mixer (blue features) and (ii) a culture chamber array comprising five parallel units. Each level of the mixer was

dimensioned to ensure efficient cell mixing from the two main inlets (A1, A2). To this aim, 17, 21 and 27 HB units were sequentially integrated on top of the fluidic channel in levels 1, 2 and 3 of the SDG, respectively. Stoichiometric mixtures of cells were generated from two main inlets (A1-A2) and delivered to downstream culture units (b). Each arrayed culture unit consisted of 10 fluidically connected culture chambers in series that included a lateral seeding channel. Two additional inlets (B1-B2), providing a flow by-pass for the device, facilitated the medium change operations.

Final device layouts (Fig.2 and Fig.S11) were drawn in CAD software (AutoCAD, Autodesk Inc.) and consisted of two layers: (i) a 100 μm thick layer for fluidic channels and chambers (Fig.2, black features) and (ii) a 36 μm thick layer for the HB structures, positioned on the top of the previous channel (Fig.2, blue features). Each layer was printed at high resolution on a chrome mask, subsequently used to prepare silicon wafer masters using photolithography. SU8-2050 and SU8-2025 negative tone photoresists were used for the first and second layers, respectively. Feature height was confirmed by optical surface profilometry (Veeco NT1100). Modifications to the master to reduce it to only the 100 μm thick layer was also developed to produce control devices.

Microfluidic devices were obtained via soft lithography³³ by replica molding of the master SU8 mold with polydimethylsiloxane (PDMS; Sylgard[®] Dow Corning Midland, MI). Briefly, PDMS was cast on the master mold in a ratio 10:1 w/w (pre-polymer to curing agent), degassed and cured at 80 $^{\circ}\text{C}$ for 3hr. After baking, devices were cut out and peeled off the SU-8 device master. Input and output ports were achieved using a 0.75mm biopsy puncher (Harris Uni-CoreTM). The PDMS layer was finally plasma treated (Plasma Cleaner, Harrick Plasma, 20s, 10W, 380mTorr O₂) and bonded to a cleaned (acetone, isopropanol, nitrogen) 50x75x1mm microscope slide (Proscitech, Thuringowa, Australia). Microfluidic devices were then sterilized by autoclaving (121 $^{\circ}\text{C}$, 20 min, wet cycle), dried overnight at 80 $^{\circ}\text{C}$ and stored until used.

Soluble species mixing validation

The mixing efficiency of soluble species within the cell mixing element (HB device) was experimentally validated for Re 1 and compared to that obtained through the equivalent purely diffusive SDG (control device featuring non-grooved channels). In detail, a solution of 20 mg/ml bovine serum albumin (BSA, Sigma) in dH₂O was pumped from the A2 inlet at a flow rate of 25 $\mu\text{l}/\text{min}$ whereas dH₂O was pumped through A1 at the same flow rate. After the establishment of steady state conditions, samples of each dilution were collected from the outlets (n=3) and the BSA concentration was measured by means of a BCA Protein Assay kit (Pierce, Thermo Fisher Scientific), following the manufacturer's instructions.

Non-diffusive particle mixing validation and microparticle image velocimetry (μPIV) analysis

The partition and extent of mixing of non-diffusive particles (mimicking a cell) within the cell mixer (HB device) was evaluated by means of microparticle image velocimetry (μPIV) analysis, assessing fluid flow profiles at each bifurcation (Re=1), and the results were compared with the equivalent

purely diffusive SDG (control device). For these measurements, a suspension of red fluorescent particles of mean diameter 2 μm was seeded from inlet A1, while dH₂O was pumped in A2. A TSI PIVCAM 13 – 8 CCD (1280 x 1024 pixel resolution) camera synchronized with a dual-head Nd:YAG pulse laser was used to obtain sequential images. For each SDG intersection, 50 images were captured at 25fps. As a measurement of the particle concentration, the intensity of the area occupied by particle trajectories was quantified in the regions corresponding to the five SDG outlets. Values were finally normalized for the 100% inlet intensity (A1).

Cell culture

A mouse embryonic fibroblast cell line (NIH-3T3) and a primary osteogenic sarcoma human cell line (SAOS2) were cultured until 80% confluent, according to the recommendation of the supplier, in Dulbecco's modified Eagle's medium, high glucose (Gibco, Australia) supplemented with 10% Fetal Bovine Serum (FBS), penicillin (100 units/mL) and streptomycin (100 $\mu\text{g}/\text{mL}$) (Gibco, Australia). Human bone-marrow derived mesenchymal stromal cells, hMSCs (Donor 8006, Lonza, Switzerland), were seeded at 4000 cells/cm² and cultured until 80% confluent in maintenance medium (MM), consisting in Dulbecco's modified Eagle's medium, low glucose supplemented with 10% Fetal Bovine Serum (FBS), penicillin (100 units/mL) and streptomycin (100 $\mu\text{g}/\text{mL}$) (Gibco, Australia). Medium was changed twice a week and hMSCs were used between P5 and P6 for all experiments.

Cell mixing validation

Cell mixing was assessed by seeding fluorescently labeled NIH-3T3 cells within both HB and control devices. Before cell seeding, devices were submerged in sterile PBS enriched with 25 $\mu\text{g}/\text{mL}$ of amphotericin B (Gibco, Australia) and degassed³⁴. Subsequently, the arrayed microbioreactors were surface-coated with extracted human fibronectin (BD Biosciences, North Ryde, Australia) at a solution concentration of 25 $\mu\text{g}/\text{ml}$ for 30mins at 37 $^{\circ}\text{C}$.

After expansions, NIH-3T3 cells were fluorescently labeled through a 10 minute incubation in culture medium enriched with 5 $\mu\text{l}/\text{ml}$ of either DiO or DiL Vybrant solution (DiD, DiL and DiO multicolor kit, Invitrogen Corporation, USA), harvested from tissue culture flasks with TrypLE Express (Gibco, Grand Island, NY) and resuspended in MM at a final concentration of 0.5x10⁶ cells/ml. A reverse color gradient was generated by seeding DiO- and DiL-labeled NIH-3T3 from A1 and A2, respectively, at a flow rate of 25 $\mu\text{l}/\text{min}$ (Re=1) through each inlet. After 1 min, the flow was stopped and cells were allowed to adhere for 4 hours in an incubator (37 $^{\circ}\text{C}$, 5% CO₂). Subsequently, cells were fixed in 4% paraformaldehyde (PFA) and their nuclei were counterstained with Hoechst. 16-bit, multi-color montage images of entire microfluidic platform were acquired using a Zeiss LSM 710 laser scanning confocal microscope and the number of red and green cells for each chamber was quantified by means of CellProfiler software³⁵.

Establishment of perfusion co-culture models of hMSCs and SAOS2 cells

The CM-MBA platform was utilized to establish hMSCs/SAOS2 osteogenic co-culture models. In detail, two different co-culture models were generated to exemplify the device: (i) a reverse gradient of hMSCs-SAOS2 and (ii) a low concentration gradient of SAOS2 seeded on equally dense monolayers of hMSCs (see Table 2).

For the first co-culture model, hMSCs (0.5×10^6 cells/ml in maintenance medium) and SAOS2s (0.25×10^6 cells/ml in maintenance medium) were co-seeded from inlets A1 and A2, respectively, at a flow rate of $25 \mu\text{l}/\text{min}$ ($Re=1$) from each inlet. For the second model, hMSCs were first seeded at a constant concentration (0.5×10^6 cells/ml in MM) through both inlets and allowed to adhere for 4 hours in an incubator (37°C , 5% CO_2). SAOS2s were then seeded on top of adherent hMSCs, by introducing SAOS2-laden medium (0.25×10^6 cells/ml) from A2 and maintenance medium from A1 (flow rates of $25 \mu\text{l}/\text{min}$). For both co-culture models, cells were allowed to adhere for 4 hours in an incubator (37°C , 5% CO_2). Devices were then either stopped immediately after seeding to assess the generation of cell ratios or placed in culture under mild continuous perfusion ($2 \mu\text{l}/\text{hr}$ to each culture unit³⁶) of either MM (control devices) or osteogenic medium (osteo devices) for 7 days. Osteogenic medium (OM) consisted of MM supplemented with 2 mM L-glutamine, 0.1 μM dexamethasone, 50 μM ascorbic acid, and 10 mM β -glycerophosphate. Static controls were also established, consisting of co-cultures of hMSCs and SAOS2s seeded with proportions matching those achieved within microbio reactors (see Table 2). Medium was changed every two days in static control plates.

Microfluidic platform endpoint analysis and imaging

At specific time points, immunofluorescence analyses were performed on the cell populations within microbio reactors. For evaluating the generation of hMSCs/SAOS2 co-culture models, six devices (three for each model) were fixed after 4 hours post seeding by applying 4% PFA for 2 min. Subsequently, a solution of 3% BSA and 0.3% Tween20 (Sigma) in PBS was injected to permeabilize cells and to block

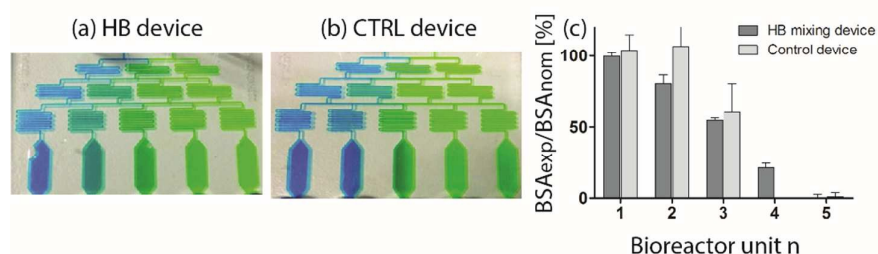
Table 2. hMSCs/SAOS2 co-culture models

Co-culture model	Microbio reactor unit	hMSCs/SAOS2
hMSCs/SAOS2 reverse gradient	1	4:0
	2	3:1
	3	2:2
	4	1:3
	5	0:4
SAOS2 low concentration gradient	1	8:0
	2	8:1
	3	8:2
	4	8:3
	5	8:4

nonspecific binding. To mark the hMSCs population, the presence of a commonly utilized surface antigen marking hMSCs, Cluster of Differentiation 73 (CD73) was detected by applying 10 $\mu\text{g}/\text{ml}$ of Mouse Anti-CD73 (Abcam) primary antibody for 1 hour, followed by the appropriate secondary antibody. Hoechst was used to stain all cell nuclei, acting as a counterstain for SAOS2 cells.

At the endpoint of each co-culture experiment (7 days), devices were washed once with PBS and fixed/permeabilized with ice cold 70% v/v ethanol for 15 min, then washed once more with PBS. An ELF97 Endogenous Phosphatase Detection Kit (Molecular Probes) was used to detect alkaline phosphatase activity, according to manufacturer's instructions. ELF97 working solution was applied until a yellow/green precipitate was observed for both SAOS2 and hMSC cells (typically within 5 min), after which the phosphatase activity was quenched with PBS (pH 8.0) enriched with 25 mM EDTA and 5 mM tetramisole (Sigma), and washed finally with PBS. DNA was detected with 2 $\mu\text{g}/\text{mL}$ propidium iodide and 100 $\mu\text{g}/\text{mL}$ ribonuclease A. Cell proliferation was also evaluated by applying 10 $\mu\text{g}/\text{ml}$ of Rabbit Anti-Ki67 (Abcam) for 1hr and the corresponding Goat Anti-Rabbit IgG secondary antibody for 45 min. All microbio reactors were then washed 3 times with PBS before imaging. The same procedure was followed for static plate controls. 16-bit, multi-colour montage images of entire microfluidic devices were acquired using a Zeiss LSM 710 laser scanning confocal microscope system and Zen 2008 acquisition software (Carl Zeiss).

Soluble factors mixing validation



Non-diffusive particles mixing validation

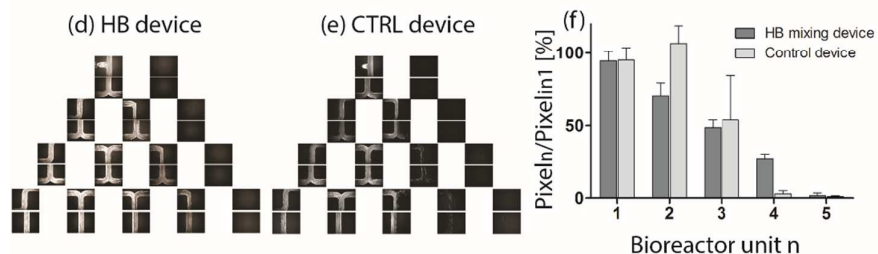


Fig.3 Characterization of HB- (a, d) and CTRL- (b, e) devices. For assessing the mixing of soluble factors, devices were perfused either with different coloured dyes (a, b) or with 20 mg/ml BSA solution and dH₂O (c) at Re=1. Quantitative measurement of BSA concentration in the 5-outlet solutions resulted in a linear trend only for the HB device, demonstrating how the presence of the HB structures significantly enhanced the mixing for high Re numbers (n=3) (c). The partition of non-diffusive particles were further visualized (d, e) and quantified (f) through microparticle image velocimetry (μ PIV) analysis, again confirming the required presence of the HB features to achieve efficient mixing of non-diffusive particles.

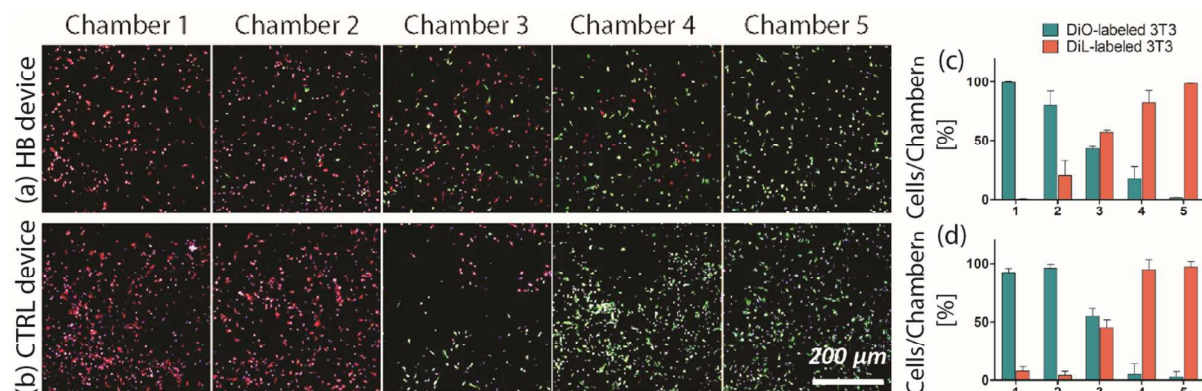


Fig.4 NIH-3T3 cells mixing validation. DiO- and DiL-labeled 3T3 were perfused from opposite inlets of devices at Re=1 and the effective mixing was evaluated at the five outlets. While linear reverse gradients were obtained for the HB device (a, c), no mixing occurred in the control device, characterized by segregation of differently labeled cells on opposite device sides (b, d). (n=3).

Results

Chaotic mixer validation: linear dilution of soluble factors and non-diffusive particles

The efficacy of the HB device in mixing both soluble factors and non-diffusive particles was experimentally assessed and compared to the control device. To quantify the performance in mixing soluble factors at high Re (qualitatively visualized by perfusing colored dyes; Fig.3a and b), bovine serum albumin (BSA) protein was dissolved in dH₂O and injected into inlet A1.

The concentration of BSA contained in the five dilutions collected from output ports matched the expected linear distribution for the HB device ($R^2 = 0.9923$) (Fig.3c). In contrast, BSA concentration measurements obtained for the purely diffusive SDG demonstrated inefficient mixing.

The partition of non-diffusive particles within consecutive levels of both chaotic- and diffusive- based SDG elements was evaluated using μ PIV analysis. Figures 3d and 3e show the reconstructed profiles of particle trajectories in the three levels of SDGs. In the HB device (Fig.3d), particles injected into inlet A1 were equally split after each level of the gradient,

giving rise to a final linear concentration gradient at the SDG outlets. Conversely, in the control purely diffusive device (Fig.3e), particles remained confined to the injection side of the device, thus following their original fluidic paths in the absence of chaotic mixing. These results were confirmed by quantification of the fluorescence intensity (Fig.3f). It is worth noting that comparable net concentration values were obtained at the central outlet (outlet 3) of both devices. However, this result is a consequence of the integral nature of the measurement. Indeed, as depicted in the μ PIV images, in the HB SDG particles are effectively spread throughout the channel width, having a homogeneous concentration corresponding to half of that upstream, whereas in the control device the channel is divided in two separated lanes (each being approximately half of the width), containing roughly 100% and 0% of the upstream concentration, respectively.

Cell mixing validation

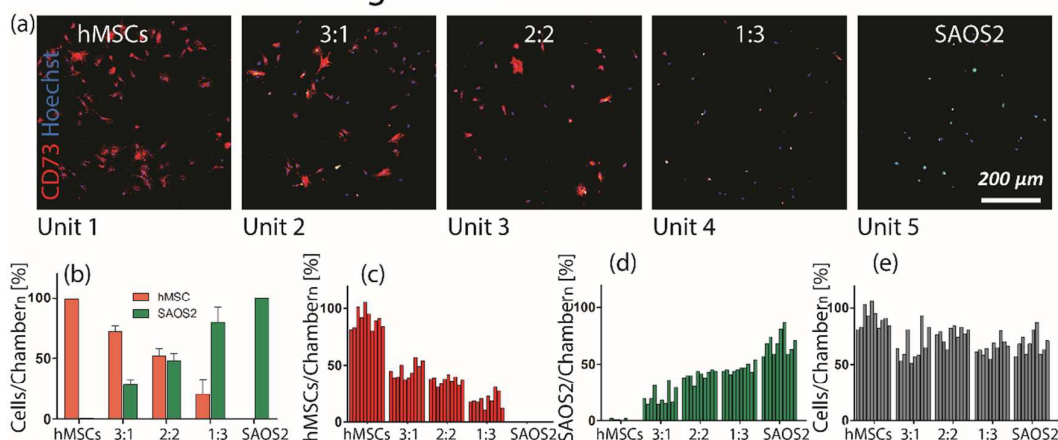
The ability to automatically mix cells was first investigated within the microfluidic platform by establishing patterns of fluorescent-labeled NIH-3T3 cells. As evidenced by fluorescence images (Fig.4a), linear reverse gradients of red and green labeled cells were achieved through the HB device. Conversely, no mixing occurred within the control device, remaining as two differently labeled cell populations segregated on opposite sides of the device (Fig.4b). These results were supported by cell quantification within the microbio reactor chambers (Fig.4c and d), confirming that only

the HB device permitted the generation of cell mixing ratios matching the expected values.

Establishment of defined hMSCs and SAOS2 osteogenic co-culture models

The cell mixer microbio reactor array platform was exploited to establish two different osteogenic co-culture models, generated through fluidically-encoded mixing of hMSCs and SAOS2 cells. For both models, the effective establishment of predicted mixing conditions (see Table 2) was assessed at day 0 within all five culture units. To quantify the final cell mixing ratios, CD73⁺ cells were identified as hMSCs³⁷. This mixing was further confirmed using hMSCs pre-labeled with DiD-Vybrant (see Supplementary Information Fig.S12). In the hMSCs/SAOS2 reverse gradient model, immunofluorescence images of cells seeded within chambers demonstrated the formation of two linear patterns within the microbio reactor in opposite directions (Fig.5a). Cell quantifications showed a good agreement of experimental ratios with the expected ones in each condition (Fig.5b). Similarly, within the second model, a linear increase of SAOS2 cells was generated (Fig.5f), with 2:1 being the highest hMSCs/SAOS2 obtained ratio (Fig.5g). The achievement of a uniform hMSCs/SAOS2 ratio within the 10 chambers of each culture unit was also assessed and confirmed for both models (Fig.5c, d, h, i). The ability to deliver an initial constant number of cells in each bio reactor chamber was also assessed. In the reverse gradient model, cells were uniformly distributed throughout the entire device

hMSCs/SAOS2 reverse gradient



SAOS2 low concentration gradient

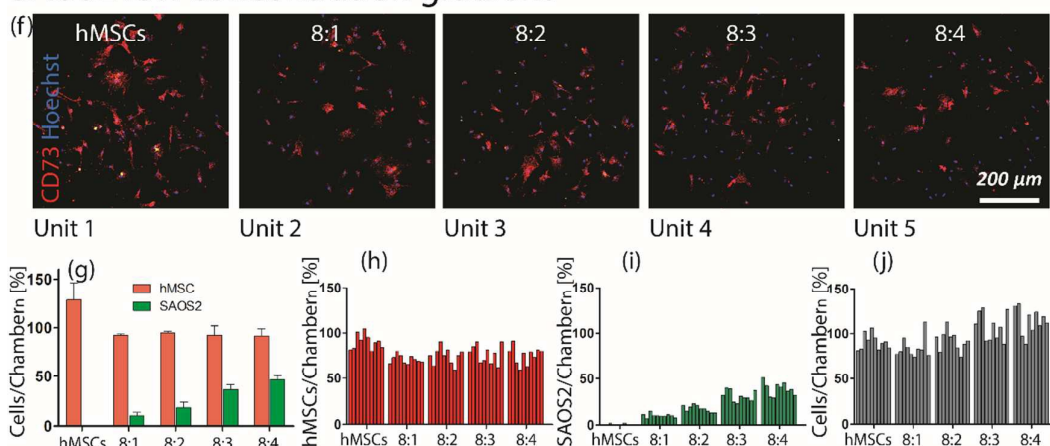


Fig. 5 Establishment of fluidically-encoded hMSCs-SAOS2 osteogenic co-culture models within the microfluidic platform. Two different models were generated: (i) a reverse gradient of hMSCs-SAOS2 (a-e) and (ii) a low concentration gradient of SAOS2 on a constant pre-established monolayer of hMSCs (f-j). Immunofluorescence images of resulting mixing ratios were acquired (a, f), in which hMSCs were identified as CD73+ cells. Quantification of cell partitioning for each culture unit confirmed the achievement of predicted mixing ratios (b, g), matching for the first model, a reverse linear gradient (from 100%MSCs to 100%SAOS2, with steps of 25%) and for the second model, a linear concentration increment of SAOS2 (from 0% to 50% at constant hMSC). In both models, cells were confirmed to be uniformly distributed throughout the entire bioreactor (e, j). (n=2).

(Fig. 5e) with an average seeding density of $59 (\pm 20)$ cells/chamber. Regarding the second model, a uniform cell distribution was achieved in the whole microbioreactor post the establishment of the hMSCs monolayers, with each culture chamber containing an average of $65 (\pm 17)$ cells. The achieved cell densities were $2830 (\pm 860)$ cells/cm² and $3145 (\pm 818)$ cells/cm², respectively, thus roughly matching the static controls (set to 3000 cells/cm²), and being comparable with preceding cell densities commonly used in osteogenic differentiation studies^{38,39}.

hMSCs-SAOS2 perfusion co-culture models: impact of SAOS2 concentration on alkaline phosphatase expression and cell proliferation

The second co-culture model, exploring the introduction of a linear increment of SAOS2 cells on a constant hMSCs

monolayer, was then used to investigate the effect of pre-osteoblastic cells on hMSCs differentiation towards the osteogenic lineage for up to 7 days. After 7 days in culture, under continuous perfusion ($2\mu\text{l/hr}$ each column) of either maintenance or osteogenic medium, microbioreactors were fixed and analyzed *in situ* both for alkaline phosphatase activity (using an ELF97 endogenous phosphatase detection kit) as a marker for early osteogenic differentiation, and Ki67 as a proliferation marker. Nuclear DNA staining (propidium iodide) was used to quantify cell number. Representative fluorescence images acquired from one entire bioreactor are shown in Figure 6, where ELF97 and Ki67 expressions are reported for both MM and OM conditions. Corresponding fluorescence levels of ELF97 (normalized for culture area) and Ki67 (normalized for the total cell number) are shown in Figure 6b, d, f, and h for each considered hMSCs/SAOS2 co-culture ratio. Both the presented images and their quantification

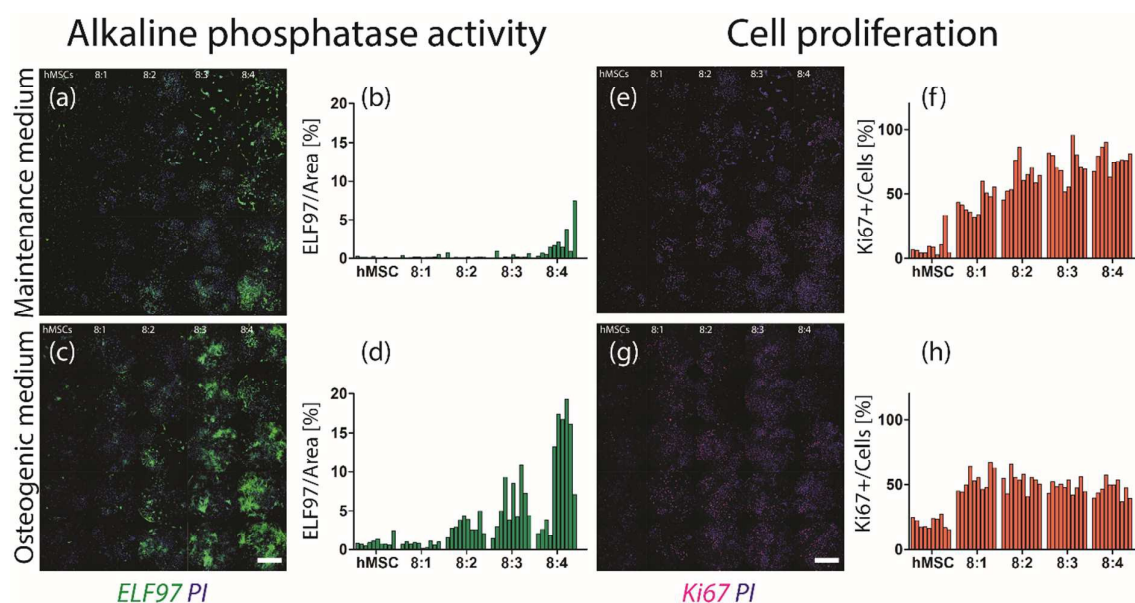


Fig.6 hMSC-SAOS2 perfusion co-culture model: impact of SAOS2 concentration on alkaline phosphatase expression and cell proliferation. Fluorescence images showing ELF97 (a, c) and Ki67 (e, g) expressions for each considered hMSC/SAOS2 co-culture ratios (8:0, 8:1, 8:2, 8:3 and 8:4), after 7 days under either maintenance (a, e) or osteogenic (c, g) medium (each column perfused at 2 μ l/hr). The shown results correspond to one bioreactor run and five representative chambers are shown for each bioreactor unit (scale bars=1mm). Corresponding fluorescence levels of ELF97 normalized for culture area (b, d) and Ki67 normalized for the total cell number (f, h) are also shown for each chamber in the bioreactor.

demonstrate the translation of the SAOS2 concentration gradient to a corresponding gradient of alkaline phosphatase expression (column groups of the bioreactor). Indeed, incremental increases of the percentage of pre-osteoblastic cells in a co-culture unit resulted in significantly higher levels of expression of ELF97, especially in the case when OM was perfused through the device, although a similar trend was observed even under MM conditions (Fig.6a). Moreover, the presence of a slight increase in ELF97 expression in subsequent downstream chambers of the same column suggest a paracrine effect from upstream chambers, as we have previously observed in our factorial microfluidic array for screening soluble factor mixtures⁴⁰. Regarding cell proliferation (Fig.6e-h), the number of Ki67⁺ cells increased with the increase in the hMSCs/SAOS2 ratio in maintenance medium, in accordance with a higher proliferation rate of the SAOS2 cell line compared to hMSCs. Conversely, the introduction of osteogenic medium under perfusion led to a plateau in cell proliferation in all co-culture conditions with SAOS2 cells (Fig.6g-h).

Individual results from the other two technical repetitions of the experiment (n=3) are also reported in Fig.SI3. Results obtained in the three replicates showed the same trend described previously for ELF97 expression, even though exhibiting differences in the absolute values mainly ascribable to variability during the staining procedures.

Discussion

In the last decade, microfluidic methodologies have been increasingly applied to the design and development of *in vitro*

models able to integrate several stimuli to better represent the cellular microenvironment, with the aim of investigating cell behavior in a controlled and reproducible way^{18, 41}. Indeed, through the reduction of dimensions down to typical cellular size-scales, fluid and mass transport phenomena become easy to control within microfluidic channels. Moreover, the length scales typical of microfluidic devices lead to highly predictable fluid dynamics, governed by a rigorous laminar flow regime⁴². These characteristics have been successfully exploited in the design of microfluidic networks able to modulate the chemical environment around cells, generating spatially defined chemical patterns by mixing soluble factors^{19, 22}. In this study, we offered a strategy to extend the potentiality of this technology to the controlled mixing of different cell types, aiming at providing a versatile and robust tool for the establishment of fluidically-encoded or programmed multicellular patterns. In this work, to overcome the diffusion limitation imposed by the absence of convective flow at the microscale, we integrated chaotic mixing features within a microfluidic resistive flow network²⁷ designed to linearly mix input fluid streams. Such grooved herringbone (HB) structures have been demonstrated to induce chaotic mixing at low Re ($0 < Re < 100$)²⁷ by division and recombination of the flow streams, thus decreasing the effective diffusion length among adjacent streamlines. Although computationally and experimentally demonstrated to provide an efficient mixing solution at the microscale^{30, 43, 44}, the exploitation of HB-based microchannels has not been previously considered for mixing live cells into defined ratios for downstream co-culture experiments. An HB mixing unit was thus designed and optimized to achieve cell mixing. By means of CFD analyses,

the mixing efficiency was correlated to the length of HB-grooved channels. CFD results demonstrated that the inclusion of HBs effectively enhanced the mixing of soluble factors within microchannels over a wide range of Reynolds numbers. The presence of HB grooves was then demonstrated to be a strict requirement for the achievement of mixing of large (microns in size) non-diffusive species, with our CFD results estimating eight as the minimum number of HB repeated units required to achieve uniform mixing in such scenarios.

Considering these requirements, a cell mixer was implemented as a stand-alone tool for generating linear patterns of non-diffusive particles in a highly controlled and automatic fashion. The efficiency of the cell mixer in sufficiently generating desired dilutions of non-diffusive particles was experimentally investigated for $Re = 1$. This Re was indeed considered a suitable compromise to achieve rapid cell seeding, thus avoiding undesired cell sedimentation or aggregation within the channels, whilst also maintaining the shear rate under a safe margin so as not to affect cell survival. μ PIV permitted visualization of the effective partition of microspheres (2 μ m in diameter) within the entire element, showing an effective equipartition of particles at each intersection. As confirmed by the quantification of particle trajectories flowing through the five outlets, the proposed technical solution permitted linear dilutions of non-diffusive species in a fast and repeatable way. As a first proof of principle, linear cell patterns were thus generated, diluting differently fluorescently labeled NIH-3T3 cells, underlining the ability to obtain fluidically-encoded mixing ratios with a precision difficult to achieve through standard manual pipetting.

The cell mixer was thereafter integrated within a microbio reactor array. The ability to establish co-culture models in a high-throughput and fully automated fashion was thus combined with the advantage of culturing cells under continuous perfusion in serially-connected micro-culture chambers. Ten serially-connected chambers (creating a column) were integrated at each of the five outputs of the cell mixer to create a microbio reactor array, capable of being inoculated with controlled cell-mixing ratios into each of the five columns.

Results obtained seeding different combinations or concentrations of hMSCs and SAOS2 demonstrated the capability of the proposed chaotic mixing SDG element to provide programmed and reliable linear patterns of cells. In particular, the establishment of two different models exemplified the versatility of this simple approach. The generation of a reverse gradient of hMSCs-SAOS2 demonstrated the ability to combine two different cell types, spatially tailoring their mixing ratios to match the specific application requirements. Furthermore, the ability to timely guide the evolution of co-culture models was also shown by delivering a linear pattern of SAOS2 on previously seeded monolayers of hMSCs.

In both hMSCs-SAOS2 models, a homogeneous cell distribution after the seeding throughout each of the microbio reactor chambers within each column ensured consistent initial culture conditions for further investigating the evolution of

these co-culture models. Proliferation and osteogenic differentiation studies were thus conducted to assess the possibility of pre-conditioning hMSCs with pre-osteoblastic cells to enhance their osteogenic regenerative potential. An increase in the activity of alkaline phosphatase (an early osteogenic marker), consistent with the initial linear distribution of SAOS2, was detected throughout the microbio reactor array, independently of the presence of osteogenic factors. Moreover, a slight increase in ELF97 expression was observed in successive downstream chambers of each microbio reactor column, suggesting the accumulation of paracrine factors induced by the continuous mild perfusion from upstream chambers. These results were also supported by the assessment of the number of proliferative cells, which was found to have an opposite trend with respect to the expression of the early osteogenic differentiation marker. A plateau in Ki67⁺ cells was indeed detected for the OM culture condition, consistent with the tendency of cells to differentiate. In the absence of osteogenic factors, on the other hand, a slight decrease in proliferating cells number was evident in successive downstream chambers of each microbio reactor column, in line with the opposite increase in ELF97 expression. Interestingly, the maximum concentration of SAOS2 tested in this model (hMSCs/SAOS2 ratio of 2:1) was enough to induce alkaline phosphatase activation after only seven days in culture, whilst expression was only slightly evident in the static macroscale control (Fig.SI4). These results suggest that the presence of small (relative) numbers of pre-osteoblastic cells could be sufficient for priming or biasing hMSCs for an osteogenic endpoint. In addition, it is worth noting that the use of a low concentration gradient of SAOS2, justified by the interest in investigating the role of small numbers of pre-osteoblastic cells on hMSCs osteogenic differentiation⁴⁵⁻⁴⁷, highlighted the suitability of the system in handling low numbers of living cells with high precision and fidelity, far beyond that possible with macroscale (pipette-based) limiting dilutions.

The establishment of the presented osteogenic hMSCs/SAOS2 co-culture models served to exemplify the potential of the detailed cell mixer microbio reactor array as a promising tool for investigating cell-cell interactions and even the dynamics of tissue patterning. It is however worth noting that whilst we have used only two cell types at five ratios, the presented platform by design is highly scalable and suitable for generating controlled co-culture models for any cell type (mammalian or otherwise (e.g. bacterial cells)) and for more than two cell types.

Conclusions

In this work, we presented a novel cell mixer microbio reactor array platform for establishing spatio-temporally tunable co-culture models through the implementation of a chaotic-based cell mixer upstream of a microbio reactor array. The computational optimization of the staggered herringbone cell mixer allowed for the effective design of a microfluidic network able to generate linear dilutions of large non-diffusive

particles, as experimentally demonstrated by means of μ PIV analyses. Upon the integration of the validated element within array of serially-connected culture chambers, the capability to split suspensions of cells into defined linear concentration patterns was confirmed, exemplifying the versatility of the system. As a final proof of principle, the validated platform was exploited as a tool for studying the interaction between pre-osteoblastic cells (SAOS2) and hMSCs through the establishment of different osteogenic co-culture models for up to seven days, providing new insight into the impacts of paracrine factor secretion and signaling on hMSCs phenotype. By design, this scalable, cell mixing, perfused microbio-reactor array has the potential to be applied to study co-culture of many cell types over a broad range of mixing ratios.

Acknowledgements

This work was partly funded by Stem Cells Australia (an Australian Research Council Special Research Initiative SR110001002) and CSIRO OCE Science Leader Fellowship (held by JCW). This work was also supported and performed in part at the Queensland node of the Australian National Fabrication Facility, a company established under the National Collaborative Research Infrastructure Strategy to provide nano- and microfabrication facilities for Australia's researchers.

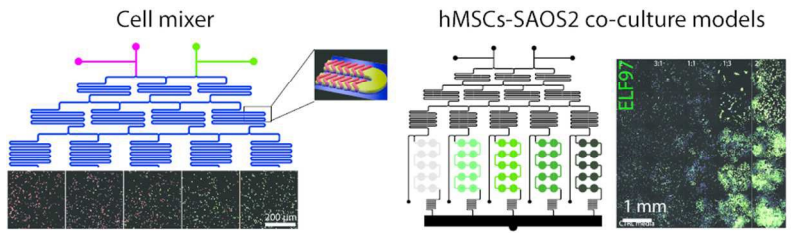
Notes and references

- I. Greenwald and G. M. Rubin, *Cell*, 1992, 68, 271-281.
- H. Rouault and V. Hakim, *Biophysical Journal*, 2012, 102, 417-426.
- Y. Wang, V. Volloch, M. A. Pindrus, D. J. Blasioli, J. Chen and D. L. Kaplan, *Journal of Tissue Engineering and Regenerative Medicine*, 2007, 1, 39-50.
- E. Walsh, Y. Ueda, H. Nakanishi and K. Yoshida, *Neurosci Lett*, 1992, 138, 103-106.
- C. Bang, S. Batkai, S. Dangwal, S. K. Gupta, A. Foinquinos, A. Holzmann, A. Just, J. Remke, K. Zimmer, A. Zeug, E. Ponimaskin, A. Schmiedl, X. K. Yin, M. Mayr, R. Halder, A. Fischer, S. Engelhardt, Y. Y. Wei, A. Schober, J. Fiedler and T. Thum, *Journal of Clinical Investigation*, 2014, 124, 2136-2146.
- J. El-Ali, P. K. Sorger and K. F. Jensen, *Nature*, 2006, 442, 403-411.
- Y. Gao, D. Majumdar, B. Jovanovic, C. Shaifer, P. C. Lin, A. Zijlstra, D. Webb and D. Li, *Biomedical Microdevices*, 2011, 13, 539-548.
- W. Liu, L. Li, X. Wang, L. Ren, X. Wang, J. Wang, Q. Tu, X. Huang and J. Wang, *Lab on a Chip*, 2010, 10, 1717-1724.
- A. M. Taylor, D. C. Dieterich, H. T. Ito, S. A. Kim and E. M. Schuman, *Neuron*, 2010, 66, 57-68.
- H. Kimura, T. Yamamoto, H. Sakai, Y. Sakai and T. Fujii, *Lab on a Chip*, 2008, 8, 741-746.
- S. N. Bhatia, M. L. Yarmush and M. Toner, *J Biomed Mater Res*, 1997, 34, 189-199.
- V. L. Tsang, A. A. Chen, L. M. Cho, K. D. Jadin, R. L. Sah, S. DeLong, J. L. West and S. N. Bhatia, *FASEB J.*, 2007, 21, 790-801.
- A. Khademhosseini, L. Ferreira, J. Blumling Iii, J. Yeh, J. M. Karp, J. Fukuda and R. Langer, *Biomaterials*, 2006, 27, 5968-5977.
- J. Fukuda, A. Khademhosseini, J. Yeh, G. Eng, J. Cheng, O. C. Farokhzad and R. Langer, *Biomaterials*, 2006, 27, 1479-1486.
- D. M. Titmarsh, H. Chen, E. J. Wolvetang and J. J. Cooper-White, *Biotechnol. J.*, 2012, 8, 167-179.
- D. Titmarsh, A. Hidalgo, J. Turner, E. Wolvetang and J. Cooper-White, *Biotechnol. Bioeng.*, 2011, 108, 2894-2904.
- P. Occhetta, M. Centola, B. Tonarelli, A. Redaelli, I. Martin and M. Rasponi, *Sci. Rep.*, 2015, 5.
- D. M. Titmarsh, H. Chen, N. R. Glass and J. J. Cooper-White, *Stem Cells Translational Medicine*, 2014, 3, 81-90.
- N. L. Jeon, S. K. W. Dertinger, D. T. Chiu, I. S. Choi, A. D. Stroock and G. M. Whitesides, *Langmuir*, 2000, 16, 8311-8316.
- K. Lee, C. Kim, B. Ahn, R. Panchapakesan, A. R. Full, L. Nordee, J. Y. Kang and K. W. Oh, *Lab on a Chip*, 2009, 9, 709-717.
- R. Sahai, C. Martino, P. Castrataro, A. Menciassi, A. Ferrari, F. Beltram and M. Cecchini, *Microelectron. Eng.*, 2011, 88, 1689-1692.
- D. Titmarsh and J. Cooper-White, *Biotechnology and Bioengineering*, 2009, 104, 1240-1244.
- V. Hessel, H. Löwe and F. Schönfeld, *Chemical Engineering Science*, 2005, 60, 2479-2501.
- H. E. H. Meijer, M. K. Singh, T. G. Kang, J. M. J. den Toonder and P. D. Anderson, *Macromolecular Symposia*, 2009, 279, 201-209.
- M. A. Unger, H.-P. Chou, T. Thorsen, A. Scherer and S. R. Quake, *Science*, 2000, 288, 113-116.
- F. Schonfeld, V. Hessel and C. Hofmann, *Lab on a Chip*, 2004, 4, 65-69.
- A. D. Stroock, S. K. W. Dertinger, A. Ajdari, I. Mezić, H. A. Stone and G. M. Whitesides, *Science*, 2002, 295, 647-651.
- S. P. Kee and A. Gavriilidis, *Chemical Engineering Journal*, 2008, 142, 109-121.
- L. Di, H. Fei, L. Yang, L. Jintian, L. Changning, S. Jiangxin and C. Ya, *Journal of Optics*, 2013, 15, 025601.
- A. D. Stroock and G. J. McGraw, *Philosophical Transactions of the Royal Society of London. Series A: Mathematical, Physical and Engineering Sciences*, 2004, 362, 971-986.
- P. Occhetta, C. Malloggi, A. Gazaneo, A. Redaelli, G. Candiani and M. Rasponi, *RSC Advances*, 2015, 5, 5087-5095.
- F. Pennella, M. Rossi, S. Ripandelli, M. Rasponi, F. Mastrangelo, M. Deriu, L. Ridolfi, C. Kähler and U. Morbiducci, *Biomedical Microdevices*, 2012, 14, 849-862.

ARTICLE

- 33 Y. N. Xia and G. M. Whitesides, *Angew. Chem., Int. Ed.*, 1998, 37, 550.
- 34 J. Monahan, A. A. Gewirth and R. G. Nuzzo, *Anal. Chem.*, 2001, 73, 3193-3197.
- 35 A. Carpenter, T. Jones, M. Lamprecht, C. Clarke, I. Kang, O. Friman, D. Guertin, J. Chang, R. Lindquist, J. Moffat, P. Golland and D. Sabatini, *Genome Biology*, 2006, 7, R100.
- 36 J. E. Frith, D. M. Titmarsh, H. Padmanabhan and J. J. Cooper-White, *PLoS ONE*, 2013, 8, e82931.
- 37 M. Dominici, K. Le Blanc, I. Mueller, I. Slaper-Cortenbach, F. C. Marini, D. S. Krause, R. J. Deans, A. Keating, D. J. Prockop and E. M. Horwitz, *Cytotherapy*, 2006, 8, 315-317.
- 38 R. McBeath, D. M. Pirone, C. M. Nelson, K. Bhadriraju and C. S. Chen, *Developmental Cell*, 2004, 6, 483-495.
- 39 N. Jaiswal, S. E. Haynesworth, A. I. Caplan and S. P. Bruder, *Journal of Cellular Biochemistry*, 1997, 64, 295-312.
- 40 D. M. Titmarsh, D. A. Ovchinnikov, E. J. Wolvetang and J. J. Cooper-White, *Biotechnology Journal*, 2013, 8, 822-834.
- 41 G. M. Whitesides, *Nature*, 2006, 442, 368-373.
- 42 C. Hansen and S. R. Quake, *Current Opinion in Structural Biology*, 2003, 13, 538-544.
- 43 J. Aubin, D. F. Fletcher and C. Xuereb, *Chemical Engineering Science*, 2005, 60, 2503-2516.
- 44 D. G. Hassell and W. B. Zimmerman, *Chemical Engineering Science*, 2006, 61, 2977-2985.
- 45 H. Kim, J. H. Lee and H. Suh, *Yonsei Med J*, 2003, 44, 187-197.
- 46 Z. Lu, S.-I. Roohani-Esfahani, G. Wang and H. Zreiqat, *Nanomedicine: Nanotechnology, Biology and Medicine*, 2012, 8, 507-515.
- 47 T. E. Rinker, T. M. Hammoudi, M. L. Kemp, H. Lu and J. S. Temenoff, *Integrative Biology*, 2014, 6, 324-337.

A Cell Mixer MicroBioreactor Array platform that permits the rapid establishment of perfused cell co-culture models in a high-throughput, programmable fashion.



102x23mm (300 x 300 DPI)